

Article

<https://doi.org/10.1038/s41467-024-51240-w>

PAK4 phosphorylates and inhibits AMPK α to control glucose uptake

Received: 9 January 2024

Accepted: 31 July 2024

Published online: 10 August 2024

 Check for updatesDandan Wu¹, Hwang Chan Yu², Hye-Na Cha³, Soyoung Park³, Yoonji Lee¹, Sun-Jung Yoon⁵, So-Young Park¹, Byung-Hyun Park¹ & Eun Ju Bae¹

Our recent studies have identified p21-activated kinase 4 (PAK4) as a key regulator of lipid catabolism in the liver and adipose tissue, but its role in glucose homeostasis in skeletal muscle remains to be explored. In this study, we find that PAK4 levels are highly upregulated in the skeletal muscles of diabetic humans and mice. Skeletal muscle-specific *Pak4* ablation or administering the PAK4 inhibitor in diet-induced obese mice retains insulin sensitivity, accompanied by AMPK activation and GLUT4 upregulation. We demonstrate that PAK4 promotes insulin resistance by phosphorylating AMPK α 2 at Ser491, thereby inhibiting AMPK activity. We additionally show that skeletal muscle-specific expression of a phospho-mimetic mutant AMPK α 2^{S491D} impairs glucose tolerance, while the phospho-inactive mutant AMPK α 2^{S491A} improves it. In summary, our findings suggest that targeting skeletal muscle PAK4 may offer a therapeutic avenue for type 2 diabetes.

p21-activated kinase 4 (PAK4), a serine/threonine kinase belonging to the group II PAK family, is ubiquitously expressed during development¹. However, its expression is specifically increased after an oncogenic transformation in many adult tissues. Notably, PAK4 is overexpressed in almost all tumors and cancer cell lines and its expression is positively correlated with poor survival rates in patients^{2,3}. Previous studies have identified PAK4 as an important player in cytoskeletal reorganization, cell proliferation and survival, and gene transcription, acting as an effector protein for Rho GTPase Cdc42 and Rac⁴.

We recently reported that PAK4 also plays a critical role in fatty acid metabolism. It achieves this mainly by phosphorylating nuclear receptor co-repressor 1 in hepatocytes⁵ and hormone-sensitive lipase and fatty acid binding protein 4 in adipocytes⁶. Mice with hepatocyte-specific *Pak4* ablation show reduced triglyceride accumulation in liver compared to their wild type counterparts when fed a high-fat diet (HFD)⁵. Similarly, when PAK4 is suppressed genetically or pharmacologically in adipocytes, a lean phenotype is observed without any changes in food intake⁶. These mice also resist adipose tissue

inflammation and glucose intolerance on a HFD. These findings suggest that PAK4, in addition to its role as an oncoprotein, regulates metabolic pathways in the liver and adipose tissues.

Skeletal muscle, which accounts for up to 80% of total glucose clearance in the body, plays a crucial role in maintaining systemic glucose homeostasis⁷. Insulin and muscle contraction are the two primary physiological stimulators of glucose uptake in skeletal muscle⁸. When insulin binds to its receptor on the cell surface of skeletal muscle, glucose transporter type 4 (GLUT4) is translocated from intracellular stores to the plasma membrane through the phosphoinositide 3-kinase (PI3K)-protein kinase B (Akt) pathway⁹. During exercise or with the presence of adiponectin, GLUT4 is also shifted to the plasma membrane through the AMP-activated protein kinase (AMPK) pathway, which operates independently of the insulin signaling pathway¹⁰. It is acknowledged that compromised GLUT4 trafficking or impaired expression, involving dysregulated transcription factors normally under the control of AMPK, is implicated in the development of insulin resistance in skeletal muscle. Consequently, the pharmacological activation of AMPK using 5'-aminoimidazole-4-

¹School of Pharmacy and Institute of New Drug Development, Jeonbuk National University, Jeonju 54896, Republic of Korea. ²Graduate School of Medical Science and Engineering, Korea Advanced Institute of Science and Technology, Daejon 34141, Republic of Korea. ³Department of Physiology, College of Medicine, Yeungnam University, Daegu 42415, Republic of Korea. ⁴College of Pharmacy, Chung-Ang University, Seoul 06974, Republic of Korea. ⁵Department of Orthopedic Surgery, Jeonbuk National University Hospital, Jeonju 54907, Republic of Korea.  e-mail: sypark@med.yu.ac.kr; bhparkut@kaist.ac.kr; ejbae7@jbnu.ac.kr

carboxamide-1-β-D-ribofuranoside, metformin, or the recently developed AMPK activators has been proposed as a strategy to overcome insulin resistance by mimicking the beneficial metabolic effects of exercise training^{11–13}. As a result, current research is increasingly focused on identifying mechanisms to regulate AMPK as a therapeutic strategy to improve insulin sensitivity. Several upstream regulators of AMPK have been identified that either positively or negatively modulate its activity. AMPK activation depends on phosphorylation of the catalytic α-subunit at T172¹⁴, primarily by liver kinase B1 (LKB1) and Ca²⁺/calmodulin-dependent protein kinase kinase¹⁵. Conversely, inhibition of AMPK is associated with phosphorylation at S485 in AMPKα1 or S491 in AMPKα2 in a variety of tissues including skeletal muscle, adipocytes and hepatocytes^{16–18}. Therefore, glucose uptake in skeletal muscle might depend on the coordinated phosphorylation of AMPKα at T172 and S485/491.

Previous studies have demonstrated the significance of Rho GTPase and F-actin remodeling in the translocation of GLUT4 stimulated by insulin^{19,20}. In a similar context, *Pak1* null mice display impaired glucose tolerance due to deficiencies in insulin-stimulated GLUT4 translocation in skeletal muscle²¹. However, no studies have been conducted to investigate the involvement of PAK4 in this process. Here, we report that PAK4 is highly upregulated in the skeletal muscles of humans and mice with diabetes. Conversely, skeletal muscle-specific *Pak4* knockout (KO) mice demonstrate improvement in insulin sensitivity, accompanied by AMPK activation and GLUT4 upregulation. This phenotype was also replicated by the treatment of a PAK4 inhibitor²² in mice. Our data reveals that PAK4 phosphorylates S485/491 of AMPKα, thereby inhibiting its activity. Accordingly, skeletal muscle-specific expression of the phospho-mimetic mutant AMPKα2^{S491D} worsened insulin resistance, while the phospho-defective mutant AMPKα2^{S491A} alleviated it, linking AMPKα2-S491 phosphorylation to the enhancement of insulin resistance. Thus, PAK4 inhibition promotes insulin sensitivity through AMPK activation, and emerges as a therapeutic target for type 2 diabetes.

Results

The expression of PAK4 is upregulated in the skeletal muscles of both diabetic humans and mice

We first explored our hypothesis that PAK4 expression is altered in skeletal muscles in diabetes. Analysis of the human skeletal muscle tissue database (GSE161721) revealed that *PAK4* mRNA levels were increased in patients with diabetes compared to healthy counterparts (Fig. 1a). We confirmed that the protein and mRNA levels of PAK4, as well as p-PAK4 (S474), was markedly upregulated in patients with type 2 diabetes mellitus (T2DM) compared to healthy controls (Fig. 1b, Supplementary Fig. 1a). Consistent with this, we observed markedly higher levels of PAK4 and p-PAK4 protein in the skeletal muscles of HFD-fed and *db/db* mice, while mRNA levels remained unchanged (Fig. 1c–e). Moreover, in line with our earlier finding that the activation of Sirt1 and protein kinase A (PKA) pathways is responsible for the protein destabilization of PAK4 in the hepatocytes and adipocytes^{5,6}, protein levels of Sirt1 and p-PKA substrates were greatly suppressed in the skeletal muscles of diabetic mice and humans (Supplementary Fig. 1b–d).

Pak4 KO mice exhibit improved glucose homeostasis

To evaluate the impact of muscle-specific PAK4 deficiency on whole body glucose homeostasis, we generated mice with a specific deletion of the *Pak4* gene in skeletal muscle. This was achieved by crossing *Pak4*^{fl/fl} mice with mice that express Cre recombinase under the control of the myosin light chain 1 promoter (*Myl1-Cre*), which is predominantly active in postmitotic type II myofibers (Supplementary Fig. 2a). The resulting *Pak4* KO mice were born in the Mendelian ratio and did not show any apparent abnormalities in appearance or behavior. Genomic PCR analysis and western blotting

confirmed the successful and specific removal of PAK4 in skeletal muscle tissues, with no changes in the expression of other PAK family members in the *Pak4* KO mice (Supplementary Fig. 2b–d). Throughout the study, littermate mice with the *Pak4*^{fl/fl} genotype were used as the wild type (WT) control.

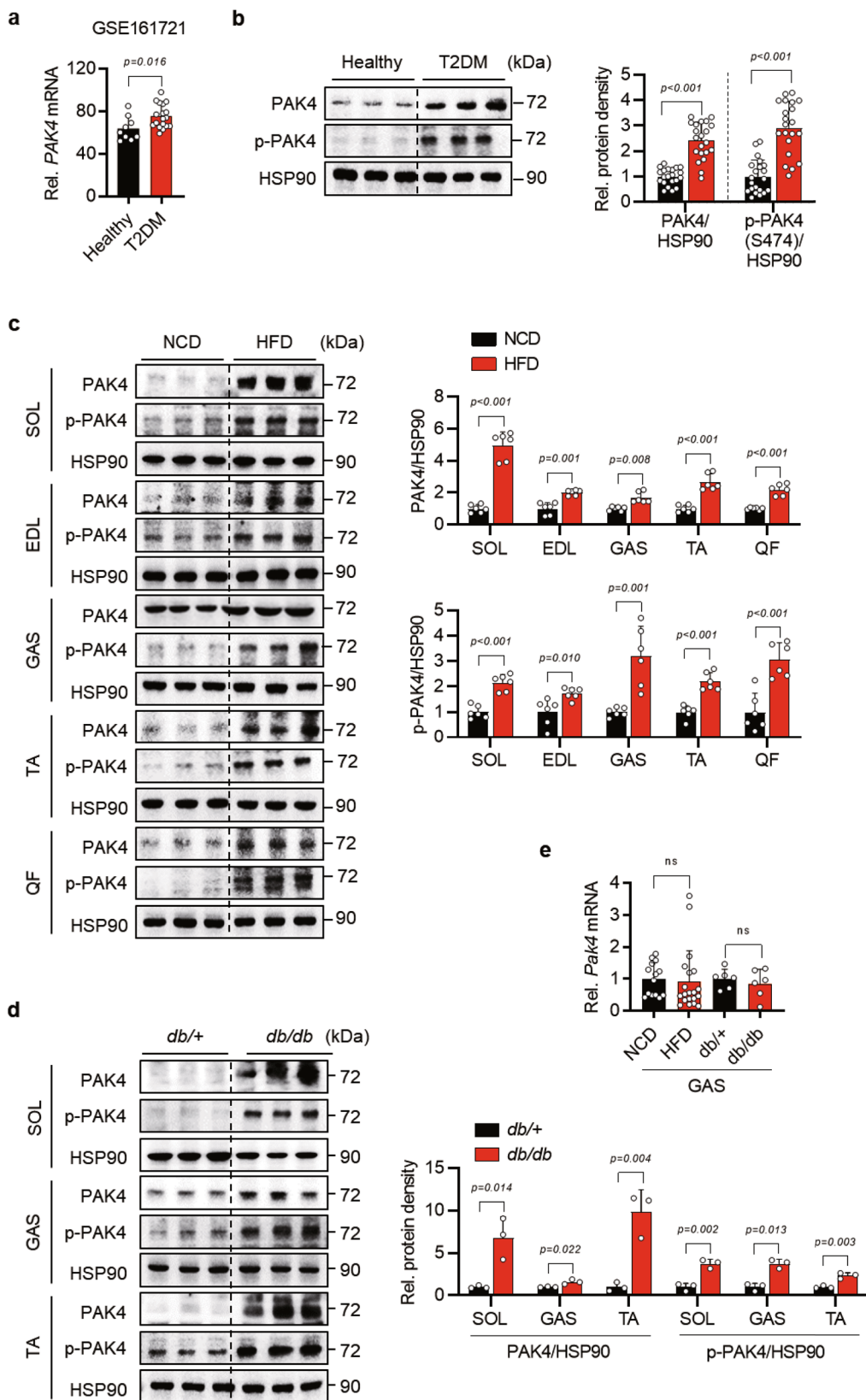
Pak4 KO and WT control male mice were placed on NCD or a HFD for 12 weeks starting at 8 weeks of age, and their metabolic profile was monitored. *Pak4* KO mice had significantly lower body weight than WT mice under HFD without any difference in food intake, and showed enhanced glucose and insulin tolerance (Fig. 2a, Supplementary Fig. 3a–c). Fasting glucose and insulin levels and HOMA-IR were significantly reduced in HFD group of *Pak4* KO mice compared to WT mice (Fig. 2b–d). Plasma adiponectin was increased but leptin levels were decreased in *Pak4* KO mice than WT mice (Fig. 2e, f). We also repeated the HFD feeding experiment in female mice, observing reduced body weight and improved glucose and insulin tolerance in female *Pak4* KO mice compared to WT mice (Supplementary Fig. 3d–g).

To confirm the enhanced glucose and insulin tolerance resulting from PAK4 deficiency, we performed hyperinsulinemic-euglycemic clamp study in a different cohort of male mice fed HFD for 12 weeks. Ablation of *Pak4* gene in skeletal muscles significantly increased the glucose infusion rate (GIR) in HFD-fed mice (Fig. 2g), indicating improved systemic insulin sensitivity. Whole-body glucose turnover and glucose uptake in the skeletal muscle were also increased in *Pak4* KO mice (Fig. 2h, i). Furthermore, under HFD condition, *Pak4* KO mice demonstrated significantly higher levels of insulin-stimulated Akt phosphorylation in skeletal muscle and epididymal adipose tissue (EAT) compared to WT mice, while no such difference was observed in the liver (Fig. 2j). These findings indicate that the absence of PAK4 in skeletal muscle improves systemic insulin resistance.

The expression and plasma membrane localization of GLUT4 is enhanced in *Pak4* KO mice

As glucose metabolism in skeletal muscle is highly influenced by GLUT4 translocation and expression^{10,23,24}, we investigated the impact of PAK4 deficiency on these factors. Through confocal microscopy and western blot analysis, we observed substantial upregulation of total and plasma membrane GLUT4 proteins in the skeletal muscles from both NCD- and HFD-fed *Pak4* KO mice compared to WT muscles (Fig. 3a, b, Supplementary Fig. 4a). Increase in the mRNA level of the GLUT4 encoding gene, *solute carrier 2A4* (*Slc2a4*), was also observed in *Pak4* KO mice (Fig. 3c).

To further explore the underlying mechanisms, we examined the signaling pathways linked to GLUT4 translocation or expression, including AMPK and p38 MAPK^{24–26}. The phosphorylation of AMPKα-T172 and its canonical substrates such as ACC, Raptor, TBC1D1, and ULK1 was significantly increased by PAK4 deficiency (Fig. 3d, Supplementary Fig. 4b). The increase in p-p38 MAPK was also noted in *Pak4* KO mice, with no alteration in the phosphorylation of its primary activating kinases, MKK3/6 (Fig. 3d, Supplementary Fig. 4b). We wondered how *Pak4* deficiency resulted in AMPK activation. Notably, the inhibitory phosphorylation of AMPK (i.e., p-AMPKα1-S485/AMPKα2-S491)²⁷, was significantly suppressed in *Pak4* KO mice compared to WT mice, whereas LKB1, the upstream regulator of AMPK¹⁵, remained unchanged across the different groups (Fig. 3d, Supplementary Fig. 4b), suggesting the possibility of PAK4 phosphorylation and inhibition of AMPK activity. We also examined whether insulin-stimulated phosphorylation of p-AMPKα1-S485/AMPKα2-S491¹⁸ was affected by *Pak4* deficiency. We found that insulin-induced a substantial increase in these phosphorylations, but this was significantly reduced in *Pak4* KO mice under both NCD and HFD conditions, suggesting crosstalk between insulin/Akt and PAK4 in the phosphorylation of AMPKα at S485/491 (Supplementary Fig. 4c). In contrast, the levels of p-AMPKα-T172 and p-p38 MAPK were higher in *Pak4* KO mice



compared to WT mice. The levels of GLUT4 in the plasma membrane and p-TBC1D4 (T649) largely mirrored those of p-Akt shown in Fig. 2j (Supplementary Fig. 4c).

We further examined the key transcription factors responsible for *Slc2a4* gene transcription. As shown in Fig. 3d and Supplementary Fig. 4d, the nuclear expression of MEF2A, Krüppel-like factor KLF15,

and GLUT4 enhancer factor (GEF, also known as SLC2ARG) was consistently upregulated in *Pak4* KO mice compared to WT mice. These findings suggest that PAK4 may inhibit AMPK α activity through phosphorylation at S485/491, thereby impeding glucose uptake by affecting both the transcription and membrane trafficking of GLUT4.

Fig. 1 | Expression of PAK4 in skeletal muscle in subjects with diabetes.

a Genotype tissue expression analysis of human skeletal muscle tissues (GSE161721, $n = 9$ for healthy and $n = 18$ for T2DM). **b** PAK4 and p-PAK4 (S474) protein levels were compared between skeletal muscles from healthy ($n = 21$) and patients with diabetes ($n = 21$). **c, d** Skeletal muscles from 8-week-old male C57BL/6 mice fed either a normal chow diet (NCD) or a 60% high-fat diet (HFD) for 12 weeks (**c**, $n = 6$) or from 16-week-old male *db/db* mice (**d**, $n = 3$) were subjected to western blotting

analysis. Protein density was quantified. **e** *Pak4* mRNA levels in gastrocnemius (GAS) muscle of HFD-fed and *db/db* mice were determined by qPCR ($n = 14$ for NCD, $n = 20$ for HFD, and $n = 6$ for *db/+* or *db/db*). Data are presented as the mean \pm SD. Unpaired two-tailed *t* test was conducted for statistical analyses (**a–e**). Source data are provided as a Source Data file. T2DM, type 2 diabetes mellitus; SOL, soleus; EDL, extensor digitorum longus; TA, tibialis anterior; QF, quadriceps femoris; ns, not significant.

PAK4 inhibits AMPK activity by phosphorylating AMPK α 2 at S491

To test our hypothesis that PAK4 might directly phosphorylate AMPK α , we conducted a series of experiments. Overexpression of HEK293T cells with AMPK α 2, a predominant form of α subunit in skeletal muscle²⁸, in combination with PAK4 resulted in co-immunoprecipitation in kinase active group (FLAG-PAK4) but not in kinase inactive group (FLAG-PAK4^{S474A}) (Fig. 4a). Direct interaction between AMPK α 2 and PAK4 was confirmed by proximity ligation assay (PLA) (Fig. 4b, Supplementary Fig. 5a). Moreover, PAK4 induced a marked increase of serine phosphorylation of AMPK α 2 while completely inhibiting threonine phosphorylation (Fig. 4a). Western blot results of p-AMPK α 2 at S491 and T172 in cell lysates correlated with the p-Ser and p-Thr in AMPK α 2 immunoprecipitates, respectively (Fig. 4a). The activation of known upstream kinases for AMPK α , i.e., its threonine kinase LKB1 and serine kinases such as p70 S6 kinase 1²⁹ and Akt^{16,18}, was not affected by PAK4 (Supplementary Fig. 5b). The physical interaction of PAK4 with AMPK α , along with its serine phosphorylation, were recapitulated in the muscles of HFD mice and type 2 diabetes patients (Supplementary Fig. 5c).

We next conducted a cell-free in vitro phosphorylation study using the recombinant human AMPK α 2 β 2 γ 1 heterotrimeric complex. The results indicated that PAK4 clearly increased p-AMPK α 2-S491 while concurrently reducing T172 phosphorylation (Fig. 4c). This finding was further corroborated by a molecular modeling study (Fig. 4d). Structural information³⁰ and disorder predictions for AMPK α 2 suggest that S491 is located within a disordered loop region of approximately 50 residues. Therefore, we hypothesize that this flexible loop could adopt a suitable conformation at PAK4's binding site to facilitate phosphorylation. The most likely conformation was predicted for the 15-mer peptide, including the S491 residue of AMPK α 2, at the substrate binding site of PAK4. The model revealed a direct interaction between PAK4 and AMPK α 2 with reliable energetic stability and structural complementarity. This interaction underpins the mechanistic insights into the PAK4-AMPK α 2 interface and supports that the phosphorylation of AMPK α 2-S491 by PAK4 is structurally feasible. The proximity of AMPK α 2-S491 to PAK4-S474 further substantiates the molecular plausibility of this phosphorylation event.

We then aimed to determine whether introducing a phospho-deficient mutant AMPK α 2, wherein S491 was replaced with alanine (AMPK α 2^{S491A}), could negate the inhibitory effect by PAK4 on AMPK activation. The PAK4-mediated increase in the p-AMPK α 2-S491, decreases in the p-AMPK α -T172, p-ACC and p-p38 MAPK, and suppression of insulin signaling were all abolished in the cells over-expressing AMPK α 2^{S491A} (Fig. 4e, f and Supplementary Fig. 5d). These findings highlight the importance of AMPK α 2-S491 phosphorylation by PAK4 in suppressing AMPK activity and affecting insulin sensitivity.

Analysis of the human skeletal muscle tissue GTEx database revealed that PAK4 was negatively correlated with genes related to mitochondrial oxidative phosphorylation, the calcium pathway, and muscle contraction (Supplementary Fig. 6a). KEGG pathway analysis also indicated involvement in multiple pathways containing AMPK (Supplementary Fig. 6b).

Skeletal muscle-specific overexpression of AMPK S491D induces glucose intolerance, while overexpression of AMPK S491A attenuates it, in mice

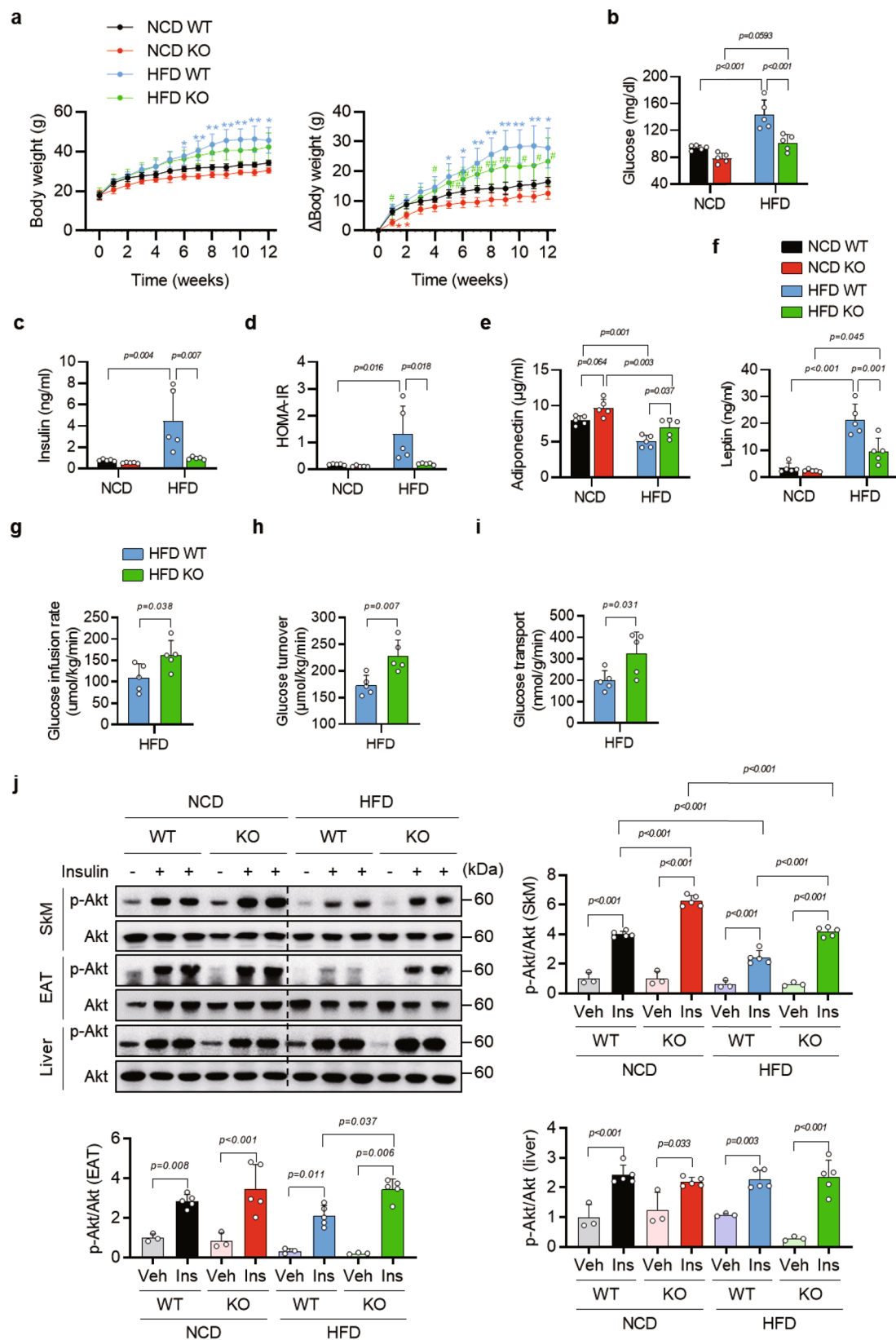
Given our discovery regarding the influence of AMPK α 2-S491 phosphorylation on PAK4-mediated suppression of AMPK activity, we were prompted to investigate its effects on systemic glucose homeostasis and insulin resistance. Eight-week old *Pak4* KO mice were fed HFD for 8 weeks and then intravenously injected with adeno-associated virus 9 (AAV9) that express either the control vector (AAV9-eGFP, eGFP), wild type AMPK α 2 (AAV9-AMPK α 2^{WT}, AMPK α 2^{WT}) or phosphomimetic mutant of AMPK (AAV9-AMPK α 2^{S491D}, AMPK α 2^{SD}) (Fig. 5a). Skeletal muscle-specific delivery of AMPK α 2 was confirmed by qPCR and western blotting (Supplementary Fig. 7a, b). Compared to AMPK α 2^{WT}, overexpression of AMPK α 2^{SD} resulted in the increases in insulin, HOMA-IR and leptin but decreased adiponectin, without changes in body weight (Fig. 5b–e, Supplementary Fig. 7c). Furthermore, GTT and ITT were aggravated in AMPK α 2^{SD} group compared to that in AMPK α 2^{WT} group (Fig. 5f, g), indicating phosphorylation of AMPK α 2 at S491 is critical for systemic insulin sensitivity. Accordingly, mice with AMPK α 2^{SD} exhibited reduction in insulin-stimulated Akt phosphorylation in both quadratus femoris and gastrocnemius muscle (Fig. 5h). The phosphorylation of ACC, Raptor, TBC1D1, ULK1, p38 MAPK, and TBC1D4 were also decreased in AMPK α 2^{SD} mice, compared to mice with AMPK α 2^{WT} (Fig. 5i, Supplementary Fig. 7d).

Conversely, we also studied whether the overexpression of phospho-inactive mutant AMPK α 2^{S491A} (AMPK α 2^{SA}) attenuates HFD-induced glucose intolerance. Four weeks after the intramuscular injection of AMPK $^{\text{SA}}$ and eight weeks of HFD feeding, mice harboring AMPK $^{\text{SA}}$ exhibited improved GTT and ITT compared to control or AMPK $^{\text{WT}}$ mice, with no changes in body weight (Supplementary Fig. 7e–g). This was accompanied by an increase in p-AMPK α -T172, p-ACC, and p-p38 MAPK in muscle (Supplementary Fig. 7h). All of these findings highlight the critical roles of the phosphorylation of AMPK α 2 at S491 in inhibiting AMPK activity and insulin sensitivity in mice.

PAK4 inhibition in L6 myotubes leads to increased glucose uptake

We next conducted experiments involving PAK4 silencing or inhibition in L6 myotubes to gain further insights into the regulatory role of PAK4 in glucose uptake. Both basal- and insulin-stimulated glucose uptake were enhanced by PAK4 silencing in L6 myotubes (Fig. 6a, b). Consistent with observations from *Pak4* KO mice, PAK4 silencing in L6 myotubes increased both surface and total GLUT4 protein levels, along with the phosphorylation of AMPK α at T172 and its downstream substrates (Fig. 6c, Supplementary Fig. 8a). Notably, PAK4 silencing reduced both basal and insulin-stimulated p-AMPK α -S485/491 while increasing p-Akt (Fig. 6c, Supplementary Fig. 8a), corroborating the results obtained from the animal data (Fig. 2j).

Further, incubation of myotubes with ND201651, a selective inhibitor of PAK4²², increased glucose uptake by alone or co-treatment with insulin (Fig. 6d). Confocal microscopy analysis confirmed the increased membrane localization of GLUT4 and glucose uptake by ND201651, which was repressed with AMPK inhibitor compound C



(CC) or p38 MAPK inhibitor SB203580 (SB) (Fig. 6e, f). To validate the significance of AMPK α in PAK4 inhibition-mediated glucose uptake, we performed AMPK α silencing experiments in L6 myotubes. When either AMPK α 1 or AMPK α 2 was silenced, the effect of ND201651 on glucose uptake was abolished (Fig. 6g). This suppression was accompanied by the decreases in the phosphorylation of AMPK α -S485/491 and p38

MAPK (Fig. 6h, Supplementary Fig. 8b). Therefore, these results, combined with the findings from the AMPK α overexpression study in vitro (Fig. 4e) and in vivo (Supplementary Fig. 7e–h), suggest that PAK4 inhibition-induced glucose uptake is mediated through the alleviation of the negative phosphorylation of AMPK α and the subsequent activation of AMPK α .

Fig. 2 | An improvement of insulin sensitivity in male *Pak4* KO mice. **a** Body weights and their changes (Δ body weight) were monitored during 12 weeks of NCD- or HFD feeding ($n=5$). $^{\circ}p < 0.05$ and $^{*}p < 0.01$ versus NCD WT; $^{*}p < 0.05$ and $^{*}p < 0.01$ versus NCD KO. **b–f** Fasting blood glucose (**b**, $n=5$), plasma insulin (**c**, $n=5$), HOMA-IR (**d**, $n=5$), adiponectin (**e**, $n=5$) and leptin (**f**, $n=5$) levels were compared among groups. **g–i** Hyperinsulinemic and euglycemic clamp experiment was performed, and glucose infusion rate (**g**, $n=5$), whole body glucose turnover rate (**h**, $n=5$), and glucose transport into skeletal muscle (**i**, $n=5$) were measured.

j Male mice were fasted for 6 h and then intravenously injected with insulin (0.75 units/kg body weight). Five or ten minutes thereafter, skeletal muscle (SkM), epididymal adipose tissue (EAT), and liver tissues were harvested for the measurement of insulin sensitivity ($n=3$ for Veh and $n=5$ for insulin treatment). Data are presented as the mean \pm SD. Unpaired two-tailed *t* test (**g–i**) and one-way ANOVA followed by Tukey's multiple comparisons test (**a–j**) were conducted for statistical analyses. Source data are provided as a Source Data file. Veh, vehicle.

PAK4 inhibitor enhances insulin sensitivity in HFD-fed and *db/db* mice

We next investigated the *in vivo* effect of ND201651. C57BL/6 mice were orally administered with ND201651 (10 and 30 mg/kg) in the final 8 weeks of a 12-week HFD feeding (Fig. 7a). Although there was a trend towards reduced body weight in ND201651 30 mg/kg group, this change did not reach statistical significance, likely due to individual variations, and food intake remained unchanged (Supplementary Fig. 9a, b). ND201651 treatment significantly improved insulin resistance, as indicated by the results of fasting glucose, insulin, HOMA-IR, GTT and ITT (Fig. 7b, c, Supplementary Fig. 9c–e). Plasma levels of leptin were also significantly decreased, while adiponectin levels were increased by ND201651 treatment (Supplementary Fig. 9f, g). Consistent with our findings in HFD-fed *Pak4* KO mice (Fig. 3a, b), ND201651 treatment increased the mRNA and protein level of GLUT4, and its plasma membrane localization, and the phosphorylation of AMPK α at T172 and its downstream substrates, while decreasing AMPK α phosphorylation at S485/491 in the skeletal muscle (Fig. 7d–f, Supplementary Fig. 9h). These findings were also demonstrated in the EAT (Supplementary Fig. 9i). Next, to rule out any potential off-target effects of ND201651 on PAK4, we repeated above experiment in *Pak4* KO mice compared to WT mice. The results from the GTT, ITT, and western blot analysis clearly indicated that ND201651 did not improve glucose intolerance in the absence of PAK4, nor did it further activate AMPK or p38 MAPK, validating the PAK4-dependent effect of ND201651 (Fig. 7g, h, Supplementary Fig. 10a, b).

Blood glucose-lowering effects by ND201651 were also demonstrated in *db/db* mice. Treatment with a 30 mg/kg dose of ND201651 significantly reduced fasting glucose and insulin levels and improved glucose and insulin tolerance (Supplementary Fig. 11a–e).

Human insulin resistance is associated with the increased PAK4 and AMPK α -S487/491 phosphorylation in skeletal muscle

Lastly, we analyzed skeletal muscle tissues from orthopedic patients with type 2 diabetes or normal glycemia to explore the relationship between PAK4 and AMPK signaling. In accordance with the previous reports^{31,32}, total and cell surface GLUT4 expression was markedly repressed in diabetes compared to normal controls (Fig. 8a, Supplementary Fig. 12a). Diabetic patients also exhibited reduced nuclear expression of MEF2A, KLF15, and GEF, consistent with GLUT4 down-regulation (Supplementary Fig. 12b). In contrast, both PAK4 protein levels and phosphorylation of AMPK α -S487/491 (human sequence, corresponding to rodent S485/491) were increased in diabetic subjects. Accordingly, the phosphorylation of AMPK α -T172 and its downstream molecules such as ACC, Raptor, TBC1D1, ULK1, and p38 MAPK was substantially decreased in the diabetic patients, consistent with previous observations³³. These results indicate that PAK4 is a bona fide kinase for AMPK α -S487/491 and plays a pivotal role in suppressing AMPK α -orchestrated GLUT4 activation in the skeletal muscles of humans (Fig. 8b).

Discussion

This study identifies PAK4 as a functional inhibitor of AMPK activity through the phosphorylation of AMPK α -S491 (α 1-S485, equivalent to S487 in humans) in both mice and human skeletal muscles.

Skeletal muscle-specific *Pak4* KO mice demonstrate AMPK activation and improved insulin sensitivity, accompanied by an increase in total- and cell surface GLUT4 expression. PAK4 inhibition enhances glucose uptake by upregulating GLUT4 transcription and increasing its membrane trafficking. These beneficial effects result from the elimination of PAK4-mediated inhibitory phosphorylation of AMPK α -S485/491.

A previous study has shown that the lack of skeletal muscle AMPK α 2 activity exacerbated HFD-induced insulin resistance³⁴. Our study is the first to demonstrate *in vivo* the critical role of AMPK α 2-S491 phosphorylation in skeletal muscle in inducing systemic glucose intolerance. We demonstrated that skeletal muscle-specific delivery of AMPK α 2-S491^{IP}, a phospho-mimetic mutant, impaired insulin sensitivity while introducing a phospho-inactive mutant improved it. This is consistent with prior *in vitro* findings that protein kinase D1 (PKD1)-mediated AMPK α 2-S491 phosphorylation impairs insulin signaling³⁵ and with a mouse study showing that serum- and glucocorticoid-induced kinase 1 (SGK1)-mediated AMPK α 1-S485 phosphorylation induces hepatic insulin resistance³⁶. As pharmacologically activating AMPK has been shown to effectively enhance skeletal muscle glucose uptake in mice and primates^{11,12,36} and diabetic patients³⁷, this study introduces a PAK4 inhibitor as a strategy for AMPK activation and a glucose-lowering agent.

It is suggested that AMPK α phosphorylation at S485/491 leads to the inhibition of AMPK α activity, either by dephosphorylation of T172 via regulating the accessibility of protein phosphatase C³⁸, or independently of T172^{18,29}. In this study, we observed that muscle-specific deletion of *Pak4* leads to a reduction in S485/491 phosphorylation of AMPK α , which was associated with an increase in T172 phosphorylation. Because the results from the cell-free *in vitro* experiments also indicated the reciprocal regulation of S491 and T172 phosphorylation in AMPK α 2, we assume that PAK4 phosphorylates S491 initially, and subsequent conformational changes could hinder phosphorylation of AMPK α 2 at T172.

Although multiple kinases, including Akt^{16,18,27}, p70 S6 kinase 1²⁹, SGK1³⁵, glycogen synthase kinase 3³⁸, PKD1³⁷, or I κ B kinase beta³⁹, have been identified as responsible for S485/491 phosphorylation of AMPK α , we demonstrate that PAK4 is an independent kinase for this residue, adding to the list of AMPK α kinases. More interestingly, insulin-stimulated AMPK α -S485/491 phosphorylation was also attenuated by PAK4 deletion *in vitro* and *in vivo*. These data suggest that Akt phosphorylation of AMPK α at S485/491 might involve PAK4 and could be context-specific, necessitating further study in the future. Overall, this study highlights the redundancy of kinases in targeting phosphorylation substrates and introduces PAK4 as a kinase accountable for AMPK α -S485/491 phosphorylation in diabetic mice.

An inverse correlation between AMPK α -S487 phosphorylation and insulin sensitivity in human muscle has been documented before, but this was analyzed only in six individuals⁴⁰. In our human study involving 42 participants, we found significantly increased levels of PAK4 and phosphorylation of AMPK α -S487/491 in the muscles of diabetic patients compared to those with normoglycemia. Surprisingly, Akt phosphorylation at S473 was not reduced but rather elevated in diabetes in our study. Many studies indicate a decrease in Akt phosphorylation in the muscle tissue of diabetic and obese animals

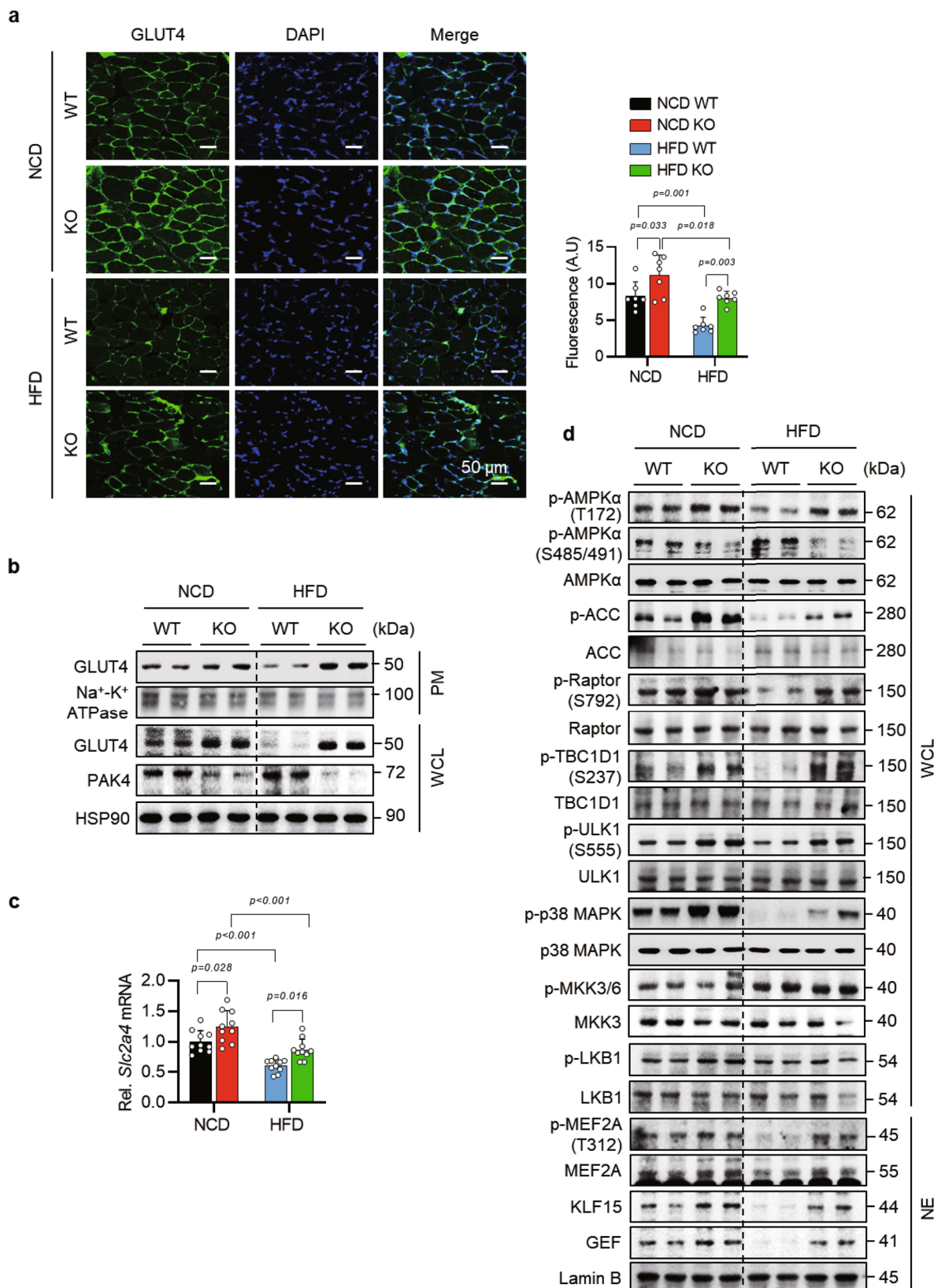
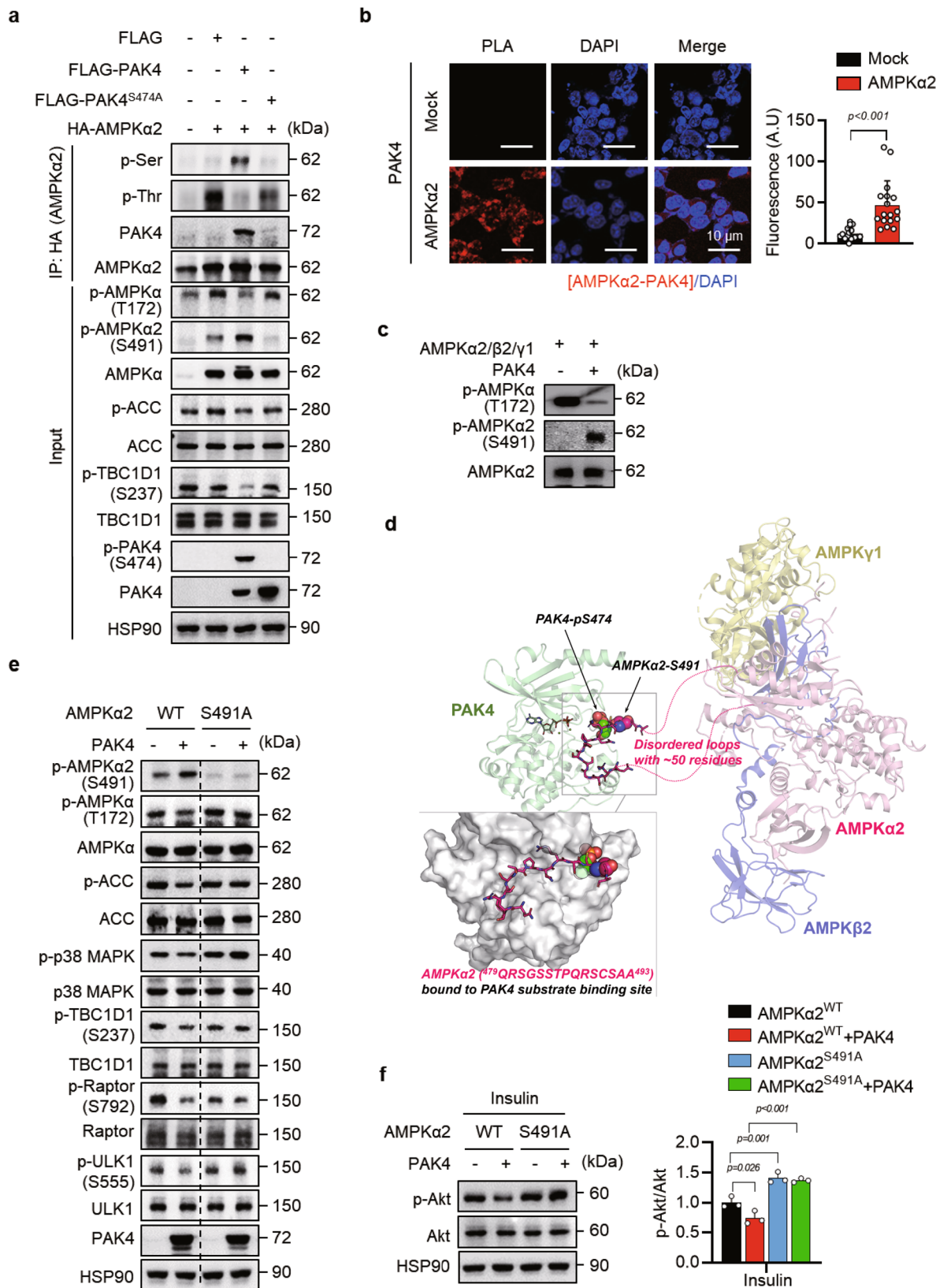


Fig. 3 | Enhancement of total and cell surface GLUT4 expression in the skeletal muscles of *Pak4* KO mice. a Immunofluorescence staining of GLUT4 in gastrocnemius muscle of 20-week-old male WT and *Pak4* KO mice fed NCD or HFD and their quantification results ($n=7$). **b** Western blot analysis of GLUT4 proteins in plasma membrane (PM) and whole cell lysate (WCL). **c** qPCR analysis for the GLUT4 encoding gene *Slc2a4* mRNA level ($n=10$). **d** Representative western blot images of

signaling molecules involved in the translocation to the plasma membrane and transcription of GLUT4 in WT and *Pak4* KO mice. Data are presented as the mean \pm SD. One-way ANOVA followed by Tukey's multiple comparisons test was conducted for statistical analysis (a, c). Source data are provided as a Source Data file. NE nuclear extract.



and humans⁴¹. Nonetheless, confirming the limited role for Akt activation for GLUT4 translocation, cellular studies suggest that Akt has little impact on GLUT4 translocation or downstream substrates phosphorylation until reduced by over 80%^{41,42}. Prior research indicates that AMPK-dependent glucose uptake represents an alternative pathway to increase glucose uptake in human muscle under conditions

of insulin resistance, as it operates independently of the insulin-Akt-mediated signaling cascade³⁷. Our discovery of significant upregulation of PAK4 and AMPK α -S487/491 phosphorylation, along with downregulation of GLUT4, in human diabetes underscores the clinical relevance of PAK4-mediated AMPK α -S485/491 phosphorylation in glucose intolerance and insulin sensitivity.

Fig. 4 | PAK4 phosphorylation of AMPK α 2 at S491 and attenuation of T172 phosphorylation. **a** HEK293T cells were transfected with the indicated plasmids, and phosphorylation of AMPK α 2 was analyzed by immunoblotting of p-Ser/Thr after immunoprecipitation (IP) with anti-HA (AMPK α 2) antibody. The main signaling pathway for AMPK activation in whole cell lysates was also shown as input. **b** After transfecting HEK293T cells as indicated, in situ proximity ligation assay (PLA) was performed to determine PAK4's direct interaction with AMPK α 2 ($n = 17$). **c** Phosphorylation of AMPK α following incubation of recombinant human AMPK α 2/β2/γ1 complex with or without recombinant PAK4 in vitro. **d** The interaction between PAK4 and AMPK α 2 was predicted by computational simulation. The structures of PAK4, AMPK α 2, AMPK β 2, and AMPK γ 1 are displayed by ribbon diagrams and colored in green, pink, blue, and yellow, respectively. The disordered loop of AMPK α 2, composed of ca. 50 residues, is depicted with pink dashed lines.

Within PAK4's substrate binding site, the bound AMPK α 2 peptide (⁴⁷⁹QRSGSSTPQRSCSA⁴⁹³) is shown in stick representation with carbon atoms colored pink. The two residues involved in phosphorylation, i.e., AMPK α 2-S491 and PAK4-pS474, are represented as spheres with their respective carbon atoms in pink and green. The ATP-Mg²⁺ is displayed in thin lines at the ATP binding site. In the bottom left inset, the molecular surface of PAK4 is shown in white.

e, f HEK293T cells were transfected with AMPK α 2 (wild type or S491A mutant) with or without PAK4 and then the basal (e) and insulin-stimulated signaling (f) were assessed by western blotting. Akt phosphorylation was assessed after insulin (10 nM) treatment for 30 min and quantification was shown ($n = 3$). Data are presented as the mean \pm SD. Unpaired two-tailed *t* test (b) and one-way ANOVA followed by Tukey's multiple comparisons test (f) and were conducted for statistical analyzes. Source data are provided as a Source Data file.

We also observed that, throughout all the different contexts of either overexpression or inhibition/deletion of PAK4, phosphorylation of p38 MAPK was negatively regulated by PAK4 and was in parallel with AMPK α -T172 phosphorylation. Additionally, PAK4 inhibitor-mediated GLUT4 translocation and glucose uptake were attenuated by the p38 MAPK inhibitor SB203580 (Fig. 6e, f). p38 MAPK has been studied as one of the signaling pathways that adapt skeletal muscle to various pathophysiological environments such as exercise, obesity, and diabetes⁴³. While p38 MAPK is beneficial in promoting glucose uptake during exercise and positively correlated with AMPK activity^{44,45}, it has been reported to mediate insulin resistance in contrast during the development of obesity-associated metabolic syndrome⁴⁶. In our human results, the marked downregulation of p38 MAPK phosphorylation in diabetes (Fig. 8a) supports the hypothesis that AMPK activation subsequently triggers downstream p38 MAPK activation, thereby reducing insulin resistance.

In contrast to *Pak4* KO mice, *Pak1* null mice exhibit deficient skeletal muscle GLUT4 translocation following insulin stimulation, resulting in peripheral insulin resistance²¹. Recent data indicate that PAK1 functions downstream of Rac1 in muscle cells, with *Rac1* KO mice also showing defective GLUT4 translocation⁴⁷. Since PAK4 is also a downstream effector of Rac1⁴⁸ and plays a role in vesicle trafficking/fusion, the reasons behind this discrepancy are unclear. Notably, *Pak1* knockout mice exhibit increased obesity⁴⁹, whereas *Pak4* KO mice display a lean phenotype compared to their wild type counterparts⁶. These contrasting roles of PAK1 and PAK4 in skeletal muscle glucose disposal, along with their comparable expression levels in skeletal muscle, highlight the need for the development of PAK4-selective inhibitors as a therapeutic strategy for type 2 diabetes.

It should be noted that there are a few limitations in this study. Firstly, we did not directly compare the glucose-lowering effect of the PAK4 inhibitor ND201651 with any other anti-diabetic drug. As an emerging therapy, the overall efficacy of a PAK4 inhibitor compared to other glucose-lowering agents will also need to be determined. Secondly, PAK4 deficiency or inhibition increased total GLUT4 expression in muscles, but the underlying mechanism of GLUT4 transcription was not completely revealed. Thirdly, this study only focused on the effect of PAK4-AMPK axis on the glucose uptake in muscle. Given the multiple beneficial effects of AMPK activation in muscle, such as increased mitochondrial biogenesis, and our previous findings indicating that the PAK4 inhibitor enhances the hepatic mitochondrial fatty acid β -oxidation⁵, it is likely that PAK4 inhibition could boost fatty acid oxidation in skeletal muscle. This would decrease intramyocyte lipid accumulation and improve muscle insulin sensitivity. Exploring this question will be a rewarding task in the development of a new anti-diabetic therapy. Lastly, we do not yet know the exact mechanism by which PAK4 ablation decreases insulin-induced phosphorylation of AMPK α -S485/491, which sharply contrasts with the increase in p-Akt. These findings imply that AMPK phosphorylation and regulation are complex and context-dependent.

In conclusion, outcomes from both gain- and loss-of-function studies affirm PAK4's role as an inhibitory kinase of AMPK, suggesting inhibition of skeletal muscle PAK4 holds promise as a therapeutic strategy for managing type 2 diabetes. Notably, we have recently identified that a PAK4 inhibitor exhibits anti-steatotic and anti-obesity effects⁵⁶. Thus, PAK4 inhibitor can truly improve systemic physiology in terms of energy metabolism. Considering AMPK's crucial role as a cellular energy sensor and its significant interest as a therapeutic target for various diseases, further investigations are essential to explore the broader applications of PAK4 inhibitor.

Methods

Human tissue samples

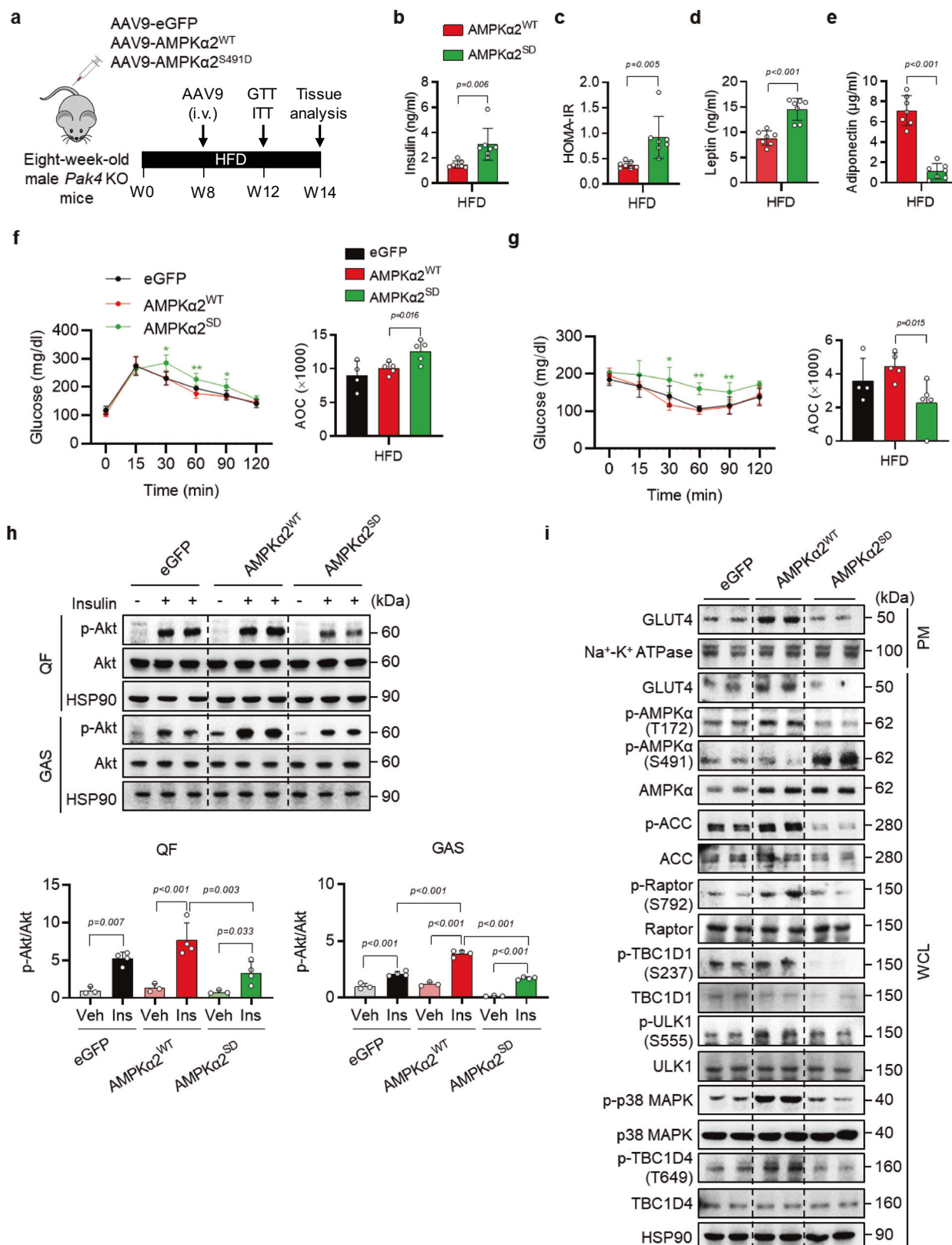
Human skeletal muscle tissue was procured during total hip arthroplasty conducted at the Orthopedic Surgery department of Jeonbuk National University Hospital (Jeonju, Korea), spanning from May 2022 to September 2023. They fasted overnight prior to undergoing surgery. Among the 42 human muscle tissues collected, 21 were from normoglycemic donors and 21 were from type 2 diabetes patients (Supplementary Table 1). During the direct anterior approach for total hip arthroplasty, the tensor fascia lata muscle was exposed and biopsy was collected for western blotting analysis. All biopsies were promptly frozen in liquid nitrogen and stored at -80°C . All patients granted written informed consent. The study was conducted according to the Declaration of Helsinki and the protocol was approved by the Institutional Review Board of Jeonbuk National University Hospital (Permit No: JBUH 2022-05-052).

Animals

Pak4^{fl/fl} mice (#015828, B6.129S2-*Pak4*^{fl/fl}Am2.1Amin/J) and *Myl1*-Cre mice (#024713, *Myl1*^{tm1cre}sjb/J) were obtained from the Jackson Laboratory (Bar Harbor, ME, USA) and crossed to generate skeletal muscle-specific *Pak4* knockout mice (*Pak4*^{fl/fl}; *Myl1*-Cre). For genotyping, tail tips were incubated with STE buffer (0.2% SDS, 100 mM Tris, 5 mM EDTA, and 200 mM NaCl, pH 7.4) and 0.5 mg/ml proteinase K for 12 h at 56°C after which they were subjected to a two-step PCR with specific forward (5'-GATGCAACGAGTGATGAG-3') and reverse (5'-TCGGCTATACGTAACAGG-3') primers. Amplification of a 496-bp band confirmed the *Pak4* genotype.

Eight-week-old male *Pak4* KO mice and WT littermates (*Pak4*^{fl/fl}) were given either an NCD (SAM #31, Samtako, Osan, Korea) or a 60% HFD (#D12492, Research Diets, New Brunswick, NJ, USA) *ad libitum* for a duration of 12 weeks. Food intake and body weight were monitored every week throughout the experiments with free access to water.

Intraperitoneal glucose tolerance tests (1 g/kg of body weight) and intraperitoneal insulin tolerance tests (0.75 U/kg of body weight) were conducted on mice after an overnight fast or a 6-hour fast, respectively. Tail vein blood glucose levels were measured using a handheld glucometer (Roche Diagnostic, Indianapolis, IN, USA) at baseline and at 15, 30, 60, 90, and 120 min after the glucose or insulin challenge. The data were subsequently graphed as baseline-



corrected area-of-the-curve (AOC) as previously suggested⁵⁰. For the in vivo measurement of Akt phosphorylation, mice were intravenously injected with insulin (0.75 units/kg body weight) and tissue samples were collected after 5 min (liver) or 10 min (EAT and skeletal muscle).

To suppress PAK4 in vivo, male C57BL/6 mice were treated with the PAK4 inhibitor ND201651 after 4 weeks of HFD feeding

until the culmination of the study. Meanwhile, seven-week-old male *db/db* mice received ND201651 through oral gavage for 8 weeks with NCD.

Mice were housed in a controlled barrier facility with a 12-hour light/dark cycle, 23 ± 1 °C temperature, and 60–70% humidity. All experimental procedures were approved by the Institutional Animal Care and Use Committees of Jeonbuk National University (Permit

Fig. 5 | Development of systemic insulin resistance by skeletal muscle-specific overexpression of AMPK α 2^{S491D}. **a** Schematic diagram of the experimental protocols. Male *Pak4* KO mice fed HFD for 8 weeks were injected intravenously with adeno-associated virus 9 (AAV9) carrying eGFP (eGFP), wild type AMPK α 2 (AMPK α 2^{WT}) or phospho-mimetic mutant of AMPK α 2 (Ser491 to Asp, AMPK α 2^{SD}) and fed HFD for another 6 weeks. **b–e** Fasting levels of plasma insulin (**b**, $n = 7$), HOMA-IR (**c**, $n = 7$), leptin (**d**, $n = 7$), and adiponectin (**e**, $n = 7$) were compared in these mice. **f, g** Glucose tolerance (**f**) and insulin tolerance (**g**, $n = 4$ for eGFP and

$n = 5$ for AMPK α 2^{WT} and AMPK α 2^{SD}) and areas of the curve (AOC) were compared in mice. $^*p < 0.05$ and $^{**}p < 0.01$ versus AMPK α 2^{WT}. **h** Insulin-stimulated p-Akt level was analyzed in quadriceps femoris (QF) and gastrocnemius (GAS) muscles by western blotting ($n = 3$ for Veh and $n = 4$ for insulin treatment). **i** AMPK signaling pathways in whole cell lysates of gastrocnemius muscle were assessed by western blotting. Data are presented as the mean \pm SD. Unpaired two-tailed *t* test (**b–e**) and one-way ANOVA followed by Tukey's multiple comparisons test (**f, g**, and **h**) were conducted for statistical analysis. Source data are provided as a Source Data file.

number: JINU 2022-041) and Yeungnam University (Permit No: YUMC-AEC2022-019).

Hyperinsulinemic-euglycemic clamp

Mouse was anesthetized with an isoflurane (4% for induction and 1–2% for maintenance) and a catheter (Helix Medical, San Mateo, CA, USA) was inserted into the jugular vein. A Y-shaped connector was affixed to the jugular vein catheter to infuse glucose or insulin during the hyperinsulinemic-euglycemic clamp. Four days after cannulation, the mouse was fasted overnight and then infused with a priming dose (900 pmol/kg body weight) of human insulin (#H10210, Eli Lilly, Indianapolis, IN, USA) to raise plasma insulin levels followed by constant infusion of insulin at 24 pmol/kg/min. Somatostatin was infused at 5.5 μ mol/kg/min to suppress endogenous insulin secretion. Blood was taken from the tail vein using capillary tubes at 20-minute intervals for instant detection of plasma glucose levels, and 20% glucose was infused at varied rates to keep glucose levels constant. The final 30 min of glucose infusion rate during the clamp was determined as glucose infusion rate.

Whole body glucose turnover rate was assessed by a continuous infusion (0.1 Ci/min) of [3^3 H] glucose (#NEC-331C-3, PerkinElmer Life and Analytical Sciences, Shelton, CT, USA) during the clamps. Glucose uptake in skeletal muscle was determined by a bolus injection of 10 μ Ci 2-deoxy-D-[1^1 C] glucose (2-[1^1 C] DG) at 75 min after starting the clamp. After finishing the clamp, mouse was anesthetized with avertin and tissue samples were taken and kept at -80° C for subsequent analysis. Plasma insulin levels were assessed using an enzyme-linked immunosorbent assay (#EZRM1-13K, MERCK, Rahway, NJ, USA), and plasma levels of [3^3 H] glucose, 2-[1^1 C]DG, and 3 H₂O were determined after plasma samples were deproteinized (Tri-Carb 4910 TR, PerkinElmer Life and Analytical Sciences). Skeletal muscle samples were homogenized to assess the 2-[1^1 C]DG-6-phosphate levels and 2-DG-6-P was separated from 2-DG in supernatants using an ion-exchange column (#731-6211, Bio-Rad, Hercules, CA, USA). The whole body glucose turnover rate was calculated by the ratio of [3^3 H] glucose infusion rate [disintegrations per minute (dpm)] to the specific activity of plasma glucose (dpm/mol) during the final 30 min of the clamps. Glucose uptake in skeletal muscle was calculated from the plasma 2-[1^1 C]DG profile using MLAB (Civilized Software, Bethesda, MD) and skeletal muscle content of 2-[1^1 C]DG-6-P.

Preparation of recombinant adeno-associated viruses (AAVs)

The AAV9-AMPK $^{\text{WT}}$ (pAAV[Exp]-CMV > EGFP(ns):WPRI) and AAV9-AMPK α 2^{S491D} generated using Cre-On system were used to drive the expression of WT or mutant AMPK in the *Pak4* KO skeletal muscle cells⁶. An AAV9-eGFP was used as a control. For skeletal muscle cell-specific delivery of AMPK, *Pak4* KO mice fed HFD for 8 weeks were randomly subjected to an intravenous injection of either AAV9-eGFP, AAV9-AMPK α 2^{WT}, or AAV9-AMPK α 2^{S491D} (1.2×10^{11} viral particles per mouse). Six weeks after injection, the expression level of eGFP in various tissues was confirmed by qPCR to determine the efficacy of AAV9 delivery.

In vivo delivery of plasmid to skeletal muscle of mice

For in vivo overexpression of AMPK α 2^{S491A} in skeletal muscle, eight-week-old male C57BL/6 mice received five injections per

gastrocnemius muscle (one in the proximal area, three in the mid area and one in the distal area, avoiding veins). Each injection contained 10 μ g of mock, AMPK α 2^{WT} or AMPK α 2^{S491A} in 22 μ l in vivo-jetPEI reagent (#201-05, Polyplus Transfection, New York, NY, USA). GTT and ITT were conducted four weeks post-injection, followed by tissue analysis.

Histology

Gastrocnemius muscle tissues were placed in a 30% sucrose solution in PBS and then frozen using liquid nitrogen-cooled isopentane for embedding. Subsequently, 10 μ m-thick frozen sections were prepared, blocked with 5% goat serum at room temperature for 40 min, and stained with the primary antibody of GLUT4 (#sc-53566, Santa Cruz Biochemicals, Dallas, TX, USA) overnight at 4° C. After washing with PBS, secondary antibodies (#11001, Alexa Fluor 488-conjugated goat anti-mouse IgG1, Thermo Fisher Scientific, Waltham, MA, USA) were incubated for 40 min at room temperature. Sections were then counterstained with 4',6-diamidino-2-phenylindole (DAPI). The resulting images were visualized using an LSM510 confocal laser scanning microscope (Carl Zeiss, Oberkochen, Germany).

Biochemical analysis

Plasma levels of various analytes were determined using specific kits as per the manufacturer's instructions. The following parameters were measured: insulin (#80-INSMS-E01, ALPCO, Salem, NH, USA), leptin (#22-LEPMS-E01, ALPCO), and adiponectin (#47-ADPHUT-E01, ALPCO). A homeostasis model for insulin resistance (HOMA-IR) index was calculated from fasting plasma insulin and glucose concentrations as follows: HOMA-IR = fasting insulin (ng/ml) \times fasting glucose (mg/dl)/405.

Cell culture and transient transfection

The human embryonic kidney (HEK) 293T fibroblasts (#CRL-3216) and L6 cells (#CRL-1458) were obtained from the American Type Culture Collection (Manassas, VA, USA). Culture media were supplemented with penicillin (100 units/ml) and streptomycin (100 μ g/ml). Both cell lines were cultured in DMEM containing 10% FBS at 37° C in a humidified environment with 5% CO₂.

Differentiation of L6 cells was induced by switching to DMEM with 2% horse serum when the cells had grown to 90% confluence. Subsequently, the cells were employed for experiments after a period of 4–6 days.

For knockdown experiment, 60 pmol of siRNA targeting specific genes (siPAK4, #70584-1; siAMPK α 1, #108079-1; and siAMPK α 2, #108079-2, all from Bioneer, Daejeon, Korea) was introduced into L6 myocytes using Lipofectamine RNAiMAX (Invitrogen, Carlsbad, CA, USA). For overexpression of PAK4, AMPK α and GLUT4, HEK293T fibroblasts or L6 myocytes were transfected with 1 μ g for HEK293T fibroblasts and 2 μ g for L6 myocytes of each plasmid using Lipofectamine 3000 (Invitrogen) when the cells had grown to 90% confluence. In L6 myocytes, the media was changed to differentiation media after overnight incubation with transfection reagents and replaced every other day for 4–5 days to induce myotube formation and subjected to the subsequent experiments.

For confocal microscopy observation, L6 cells were grown in 4-well culture chamber glass bottom slides and transfected with pB-

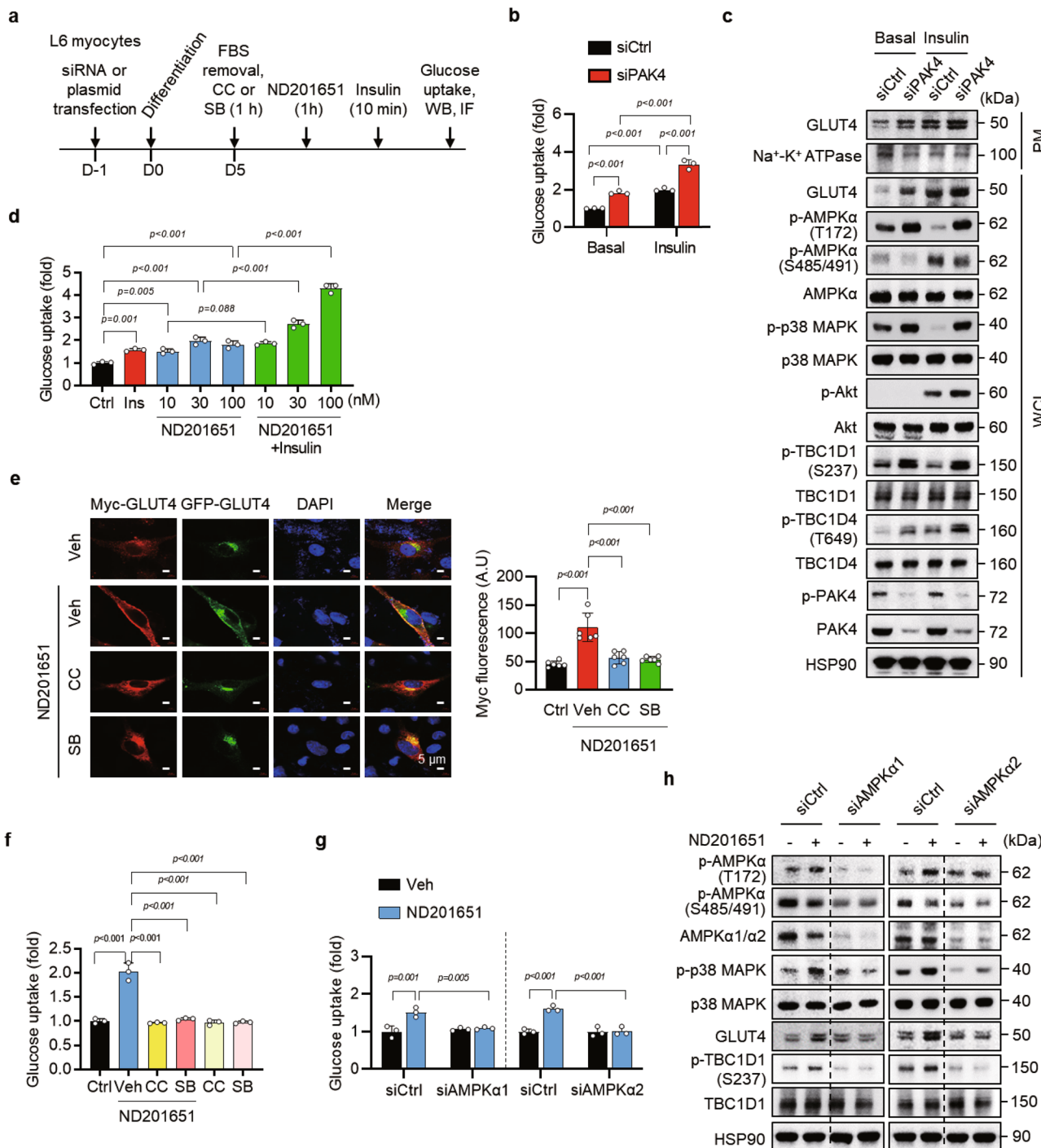


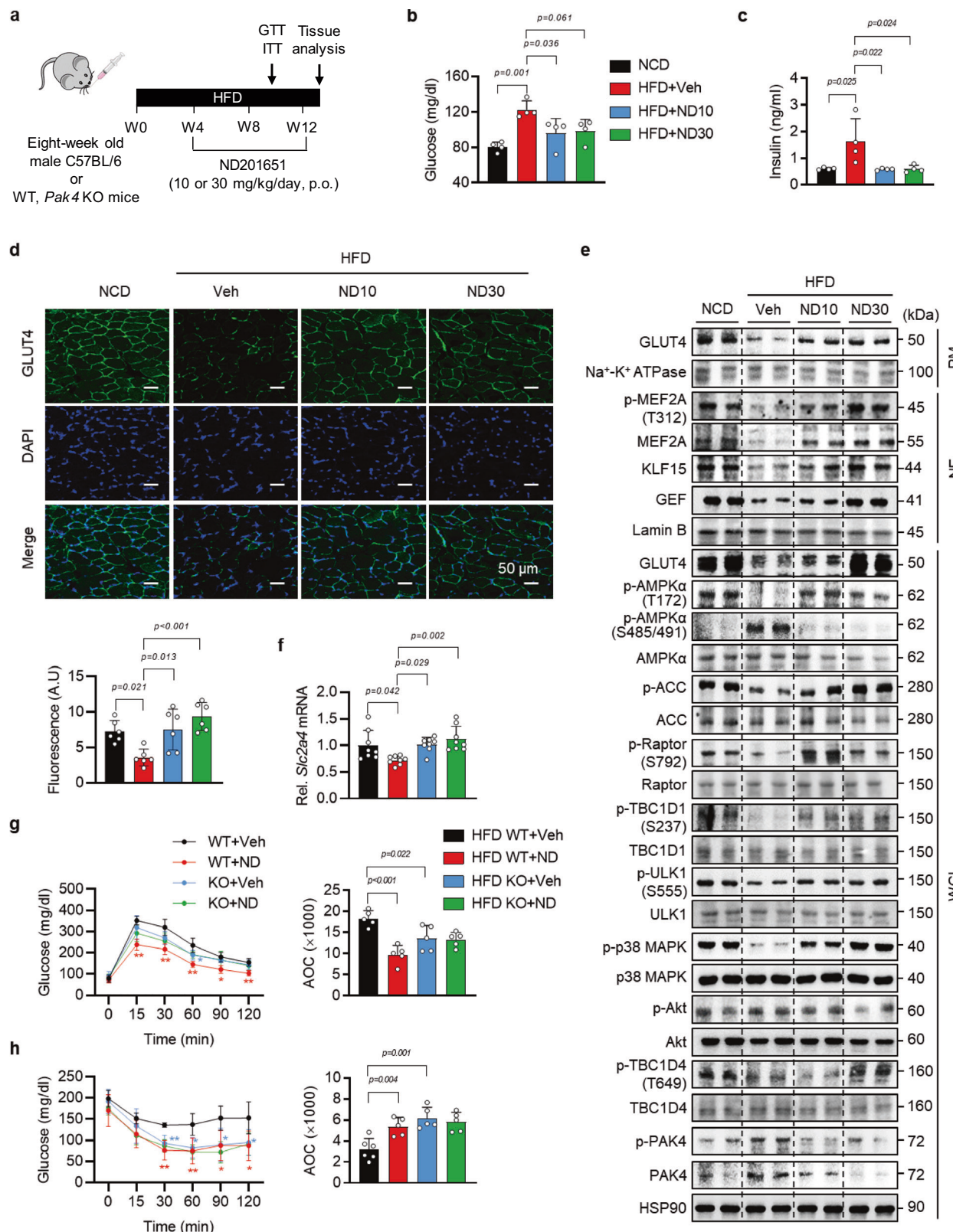
Fig. 6 | Effects of PAK4 inhibition on glucose uptake. **a–c** L6 myocytes were transfected with siRNA against PAK4 (siPAK4) or scrambled RNA (siCtrl), and then subjected to differentiation. Myotubes at day 5 were treated with 10 nM insulin for 10 min (**a**). In vitro glucose uptake (**b**) and glucose uptake-related signaling pathways (**c**) were determined in these cells ($n = 3$). **d** L6 myotubes were treated with various concentrations of PAK4 inhibitor (ND201651) alone or in the combination with 10 nM insulin for 10 min, and then glucose uptake was measured ($n = 3$). **e**, **f** L6 myotubes were treated with 100 nM ND201651 with or without 10 μ M compound C (CC) or 10 μ M SB203580 (SB). Representative confocal microscopy images of

GLUT4 localization and their quantification results (**e**, $n = 6$) and in vitro glucose uptake (**f**, $n = 3$). **g**, **h** L6 myocytes were transfected with siRNA against AMPK α 1 or 2 (siAMPK α 1 or 2) or scrambled RNA (siCtrl). Myotubes at day 5 were treated with vehicle (Veh) or 100 nM ND201651 for 1 h. In vitro glucose uptake (**g**, $n = 3$) and western blot analysis of the glucose uptake-related signaling pathways (**h**) were performed. Data are presented as the mean \pm SD. One-way ANOVA followed by Tukey's multiple comparisons test was conducted for statistical analyzes (**b**, **d**–**g**). Source data are provided as a Source Data file.

GLUT4-7myc-GFP construct (#52872, Addgene, Watertown, MA, USA). Cells were cultured for 5 days to induce myotube formation and serum deprived for 2 h before the experiment. Myc-tag antibody (#2272, Cell Signaling Technology, Danvers, MA, USA) was used to assess GLUT4 translocation.

Proximity ligation assay (PLA)

Protein interactions were assessed using a Duolink PLA kit (#DUO92002, Sigma-Aldrich, St. Louis, MO, USA) as previously described⁵. Briefly, HEK293T cells were fixed with 5% neutral buffered formalin, permeabilized with PBS/0.1% Triton X-100, and



incubated with anti-PAK4 (#sc-390507, Santa Cruz Biochemicals) in conjunction with anti-AMPK α (#5831, Cell Signaling Technology). Samples were then incubated with Duolink in situ PLA Probes (anti-rabbit Minus and anti-mouse Plus) for 1 h. Signals were amplified with polymerase using in situ Detection Reagents Green. Finally, cells were counterstained with DAPI and images were

captured using an LSM880 confocal laser scanning microscope (Carl Zeiss).

In vitro glucose uptake assay

Glucose uptake into L6 myotubes was measured using a glucose uptake cell-based assay kit (#600470, Cayman, Ann Arbor, MI, USA) according

Fig. 7 | Increases in systemic insulin sensitivity and GLUT4 activation by ND201651 in HFD-fed mice. **a** Eight-week-old male C57BL/6 mice were orally administered ND201651 (ND) once daily at a dose of 10 or 30 mg/kg for 8 weeks, while being fed either a normal chow (NCD) or high-fat diet (HFD). Fasting blood glucose (**b**, $n = 4$) and insulin (**c**, $n = 4$) levels were measured. Immunofluorescence staining of GLUT4 (**d**, $n = 6$) and the signaling pathway involved in GLUT4 expression and its translocation to the plasma membrane (**e**) in gastrocnemius muscle. **f** qPCR analysis of *Slc2a4* mRNA levels ($n = 8$). **g, h** Eight-week-old male *Pak4* KO

mice and their WT littermates were orally administered ND201651 once daily at a dose of 30 mg/kg for 4 weeks while on a HFD. Glucose tolerance (**g**, $n = 5$), insulin tolerance (**h**, $n = 5$), and the areas of the curve (AOC) were compared in these mice. $p < 0.05$ and $^{*}p < 0.01$ versus HFD WT+Veh Data are presented as the mean \pm SD. One-way ANOVA followed by Tukey's multiple comparisons test was conducted for statistical analyzes (**b-d, f-h**). Source data are provided as a Source Data file. ND10, ND201651 10 mg/kg; ND30, ND201651 30 mg/kg.

to the manufacturer's protocol. Briefly, cells were treated with the indicated drugs after a 2-hour serum starvation period. After three washes with KR buffer (HEPES 20 mM, KH_2PO_4 5 mM, MgSO_4 1 mM, CaCl_2 1 mM, NaCl 136 mM, KCl 4.7 mM, pH 7.4), cells were treated with insulin in KR buffer for 10 min, followed by incubation with NBD glucose at a concentration of 500 $\mu\text{g}/\text{ml}$ for 20 min at room temperature. The reactions were terminated by washing the cells with ice-cold KR buffer. Cells were then lysed with Mammalian Protein Extraction Reagent (#78505, Thermo Fisher Scientific) and centrifuged at 15000 \times g for 10 sec. Cell-based assay buffer was added after careful removal of the supernatant and 2-NBDG taken up by the cells was detected using a microplate reader at excitation/emission = 485/535 nm.

Cell-free in vitro phosphorylation assay

The recombinant AMPK α 2/β2/γ1 complex (0.6 μg , #SRP5003, Sigma-Aldrich) was incubated with recombinant PAK4 (0.2 μg , #ab96405, Abcam) in an assay buffer (50 mM Tris-HCl, 10 mM MgCl_2 , 2 mM DTT, 0.1 mM EDTA, and 500 μM ATP, pH 7.6) at 30 °C for 10 min. Following incubation, the reaction mixtures were analyzed by SDS-PAGE.

Prediction of PAK4-AMPK α 2 complex model

Computational simulation was conducted to predict the complex model of PAK4 and AMPK α 2. The protein 3D structure of human PAK4 (PDB id: 4XBR)⁵¹ was retrieved from the Protein Data Bank (<https://www.rcsb.org>). By using the FlexPepDock protocol in Rosetta^{52,53}, the plausible conformations of the 15-mer peptide (479QRSGSSTPQRSCSA⁴⁹³) of AMPK α 2 were modeled at the substrate binding site of PAK4. During the simulation, the number of high-resolution structures was set to 300. Among the top-scoring ten models, the most appropriate model was manually inspected and selected. The 3D structure of the human AMPK α 2/β2/γ1 complex (PDB id: 7MYJ)³⁰ was shown together in Fig. 4d. The molecular graphic figure was generated by PyMOL v.2.5.4 (Schrödinger, New York, NY, USA).

Mutagenesis of AMPK α

The human AMPK α plasmid vector mutants (#HG11488-ACG, Sino Biological, Beijing, China) was generated by site-directed mutagenesis (Cosmo Genetech, Seoul, Korea). Specifically, AMPK α 2^{S491A} and AMPK α 2^{S491D} mutants were generated by introducing a point mutation that changed the serine residue in AMPK α 2 to alanine or aspartic acid as follows: AMPK α 2^{S491A} (TCT \rightarrow GCA), AMPK α 2^{S491D} (TCT \rightarrow GAC).

Plasmid construction

The AMPK expression, driven by the CMV3 promoter, was encoded by pCMV3/AMPK-GFP. The *PRKAA2* gene was inserted into the *Kpn*I and *Xba*I sites of pCMV3 vector, which is 6.164 kb in size (#HG11488-CF, Sino Biological). The PAK4 expression, driven by the CMV3 promoter, was encoded by pCMV3/PAK4-HIS. The *PAK4* gene was inserted into the *Kpn*I and *Xba*I sites of the pCMV3 vector, which is 6.848 kb in size (#HG12175-CH, Sino Biological). The GLUT4 expression, driven by the MMLV promoter, was encoded by pB/GLUT4-7myc-GFP. The *Slc2a4* gene was inserted into the *Eco*RI and *Not*I sites of pB vector, which is 5.783 kb in size (#52872, Addgene).

Subcellular fractionation, western blotting, and co-immunoprecipitation (Co-IP)

Plasma membrane fraction was obtained using the MEM-PER membrane protein extraction kit (#89842, Thermo Fisher Scientific). L6 cells were cultured in a 100 mm culture dish or 6-well plate for isolation of membrane protein or whole cell lysate, respectively. Nuclear extracts were isolated using the NE-PER Nuclear and Cytoplasmic 590 Extraction Kit (#78835, Thermo Fisher Scientific). Tissue or cell lysates (20 μg) were then separated by 10% SDS-PAGE and transferred onto PVDF membranes. Following blocking with 5% skim milk, the blots were probed with primary antibodies.

For co-immunoprecipitations, 200 μg protein was incubated with 2 μg of primary antibodies overnight at 4 °C followed by protein G agarose (#15920-010, Invitrogen) for 2 h at 4 °C. Subsequently, the blots were probed with secondary antibodies. Immunoreactive bands were detected using a Las-4000 imager (GE Healthcare Life Science, Pittsburgh, PA, USA). Further details on the antibodies are provided in Supplementary Table 2.

RNA isolation and qPCR

Total RNA was extracted from frozen skeletal muscle or L6 myotubes using an RNA Iso kit (TaKaRa, Tokyo, Japan). The RNA was then precipitated with isopropanol, desiccated using 70% ethanol, and reconstituted in diethylpyrocarbonate-treated distilled water. First-strand cDNA was synthesized with the random hexamer primer provided in the first-strand cDNA synthesis kit (Applied Biosystems, Foster City, CA, USA). Specific primers were designed using PrimerBank (<https://pga.mgh.harvard.edu/primerbank>, Supplementary Table 3). qPCR reactions were carried out in a final volume of 10 μl , comprising 10 ng of reverse-transcribed total RNA, 200 nM of both forward and reverse primers, and PCR master mixture. The qPCR analysis was conducted in 384-well plates using the ABI Prism 7900HT Sequence Detection System (Applied Biosystems).

Statistics and reproducibility

All experiments requiring statistical analysis were performed at least three times with similar results. Data are expressed as the mean \pm standard deviation (SD). No statistical methods were used to pre-determine sample sizes, but our sample sizes are similar to those reported in previous publications^{54,55}. Data from animal and cell studies were collected in a randomized and blinded fashion, and no data were excluded during the statistical analysis. Data distribution was assumed to be normal but this was not formally tested.

For comparisons between the two groups, a Student's unpaired *t*-test was employed. Comparisons among multiple groups were performed using one-way ANOVA with Tukey's post hoc analysis for continuous variables. The exact *p*-value is indicated on the graph, and a *p*-value less than 0.05 was considered significant. IBM SPSS 27.0 and GraphPad 9.5 software were utilized for statistical analysis.

Reporting summary

Further information on research design is available in the Nature Portfolio Reporting Summary linked to this article.

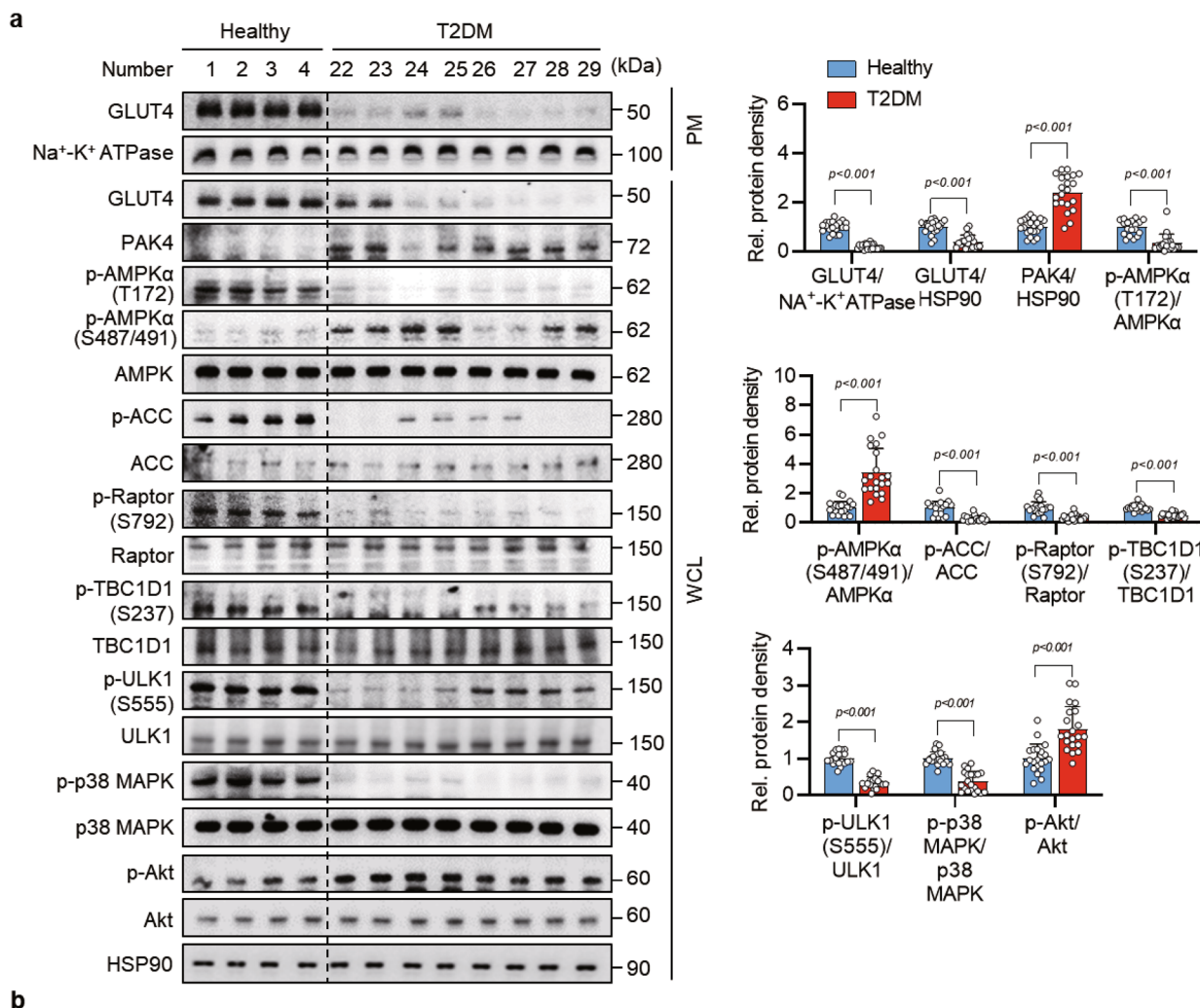


Fig. 8 | The expression of PAK4 and its downstream signaling molecules in normoglycemic individuals and type 2 diabetes patients. a Western blotting analysis was performed for the indicated proteins in skeletal muscle obtained from patients with type 2 diabetes ($n = 21$) or normoglycemic individuals ($n = 21$). **b** A

proposed model for the PAK4-mediated inhibition of skeletal muscle glucose transport. Data are presented as the mean \pm SD. Unpaired two-tailed t test was conducted for statistical analysis (a). Source data are provided as a Source Data file.

Data availability

The raw data for all bars and line graphs as well as the original uncropped western blots can be found in the accompanying files. Source data are provided with this paper.

References

- Rane, C. K. & Minden, A. p21 activated kinase signaling in cancer. *Sci. min. Cancer Biol.* **54**, 40–49 (2019).
- Callow, M. G. et al. Requirement for PAK4 in the anchorage-independent growth of human cancer cell lines. *J. Biol. Chem.* **277**, 550–558 (2002).
- Yuan, Y. et al. PAK4 in cancer development: Emerging player and therapeutic opportunities. *Cancer Lett.* **545**, 215813 (2022).
- Won, S. Y., Park, J. J., Shin, E. Y. & Kim, E. G. PAK4 signaling in health and disease: defining the PAK4-CREB axis. *Exp. Mol. Med.* **51**, 1–9 (2019).
- Shi, M. Y. et al. p21-activated kinase 4 suppresses fatty acid β -oxidation and ketogenesis by phosphorylating NCoR1. *Nat. Commun.* **14**, 4987 (2023).
- Yu, H. C. et al. p21-activated kinase 4 counteracts PKA-dependent lipolysis by phosphorylating FABP4 and HSL. *Nat. Metab.* **6**, 94–112 (2024).
- DeFronzo, R. A., Ferrannini, E., Sato, Y., Felig, P. & Wahren, J. Synergistic interaction between exercise and insulin on peripheral glucose uptake. *J. Clin. Invest.* **68**, 1468–1474 (1981).
- Goodyear, L. J. & Kahn, B. B. Exercise, glucose transport, and insulin sensitivity. *Annu Rev. Med.* **49**, 235–261 (1998).
- Chang, L., Chiang, S. H. & Saltiel, A. R. Insulin signaling and the regulation of glucose transport. *Mol. Med.* **10**, 65–71 (2004).
- Richter, E. A. & Hargreaves, M. Exercise, GLUT4, and skeletal muscle glucose uptake. *Physiol. Rev.* **93**, 993–1017 (2013).
- Cokorinos, E. C. et al. Activation of skeletal muscle AMPK promotes glucose disposal and glucose lowering in non-human primates and mice. *Cell Metab.* **25**, 1147–1159 (2017).
- Kristensen, J. M., Treebak, J. T., Schjerling, P., Goodyear, L. & Wojtaszewski, J. F. Two weeks of metformin treatment induces AMPK-dependent enhancement of insulin-stimulated glucose uptake in mouse soleus muscle. *Am. J. Physiol. Endocrinol. Metab.* **306**, E1099–E1109 (2014).
- Sakoda, H. et al. Activation of AMPK is essential for AICAR-induced glucose uptake by skeletal muscle but not adipocytes. *Am. J. Physiol. Endocrinol. Metab.* **282**, E1239–E1244 (2002).
- Crute, B. E., Seefeld, K., Gamble, J., Kemp, B. E. & Witters, L. A. Functional domains of the $\alpha 1$ catalytic subunit of the AMP-activated protein kinase. *J. Biol. Chem.* **273**, 35347–35354 (1998).
- Hardie, D. G., Ross, F. A. & Hawley, S. A. AMPK: a nutrient and energy sensor that maintains energy homeostasis. *Nat. Rev. Mol. Cell Biol.* **13**, 251–262 (2012).
- Berggreen, C., Gormand, A., Omar, B., Degerman, E. & Goransson, O. Protein kinase B activity is required for the effects of insulin on lipid metabolism in adipocytes. *Am. J. Physiol. Endocrinol. Metab.* **296**, E635–E646 (2009).
- Coughlan, K. A. et al. PKD1 Inhibits AMPK $\alpha 2$ through phosphorylation of serine 491 and impairs insulin signaling in skeletal muscle cells. *J. Biol. Chem.* **291**, 5664–5675 (2016).
- Valentine, R. J., Coughlan, K. A., Ruderman, N. B. & Saha, A. K. Insulin inhibits AMPK activity and phosphorylates AMPK Ser $^{485/491}$ through Akt in hepatocytes, myotubes and incubated rat skeletal muscle. *Arch. Biochem Biophys.* **562**, 62–69 (2014).
- Chiu, T. T., Patel, N., Shaw, A. E., Bamburg, J. R. & Klip, A. Arp2/3- and cofilin-coordinated actin dynamics is required for insulin-mediated GLUT4 translocation to the surface of muscle cells. *Mol. Biol. Cell* **21**, 3529–3539 (2010).
- Usui, I., Imamura, T., Huang, J., Satoh, H. & Olefsky, J. M. Cdc42 is a Rho GTPase family member that can mediate insulin signaling to glucose transport in 3T3-L1 adipocytes. *J. Biol. Chem.* **278**, 13765–13774 (2003).
- Wang, Z., Oh, E., Clapp, D. W., Chernoff, J. & Thurmond, D. C. Inhibition or ablation of p21-activated kinase (PAK1) disrupts glucose homeostatic mechanisms in vivo. *J. Biol. Chem.* **286**, 41359–41367 (2011).
- Mao, Y. et al. p21-activated kinase 4 inhibition protects against liver ischemia/reperfusion injury: Role of nuclear factor erythroid 2-related factor 2 phosphorylation. *Hepatology* **76**, 345–356 (2022).
- Hansen, P. A., Nolte, L. A., Chen, M. M. & Holloszy, J. O. Increased GLUT-4 translocation mediates enhanced insulin sensitivity of muscle glucose transport after exercise. *J. Appl. Physiol.* **85**, 1218–1222 (1998).
- Montessuit, C. et al. Regulation of glucose transporter expression in cardiac myocytes: p38 MAPK is a strong inducer of GLUT4. *Cardiovasc Res* **64**, 94–104 (2004).
- Hernandez, R., Teruel, T. & Lorenzo, M. Akt mediates insulin induction of glucose uptake and up-regulation of GLUT4 gene expression in brown adipocytes. *FEBS Lett.* **494**, 225–231 (2001).
- Valverde, A. M. et al. Insulin and insulin-like growth factor I up-regulate GLUT4 gene expression in fetal brown adipocytes, in a phosphoinositide 3-kinase-dependent manner. *Biochem. J.* **337**, 397–405 (1999).
- Ning, J., Xi, G. & Clemmens, D. R. Suppression of AMPK activation via S485 phosphorylation by IGF-I during hyperglycemia is mediated by AKT activation in vascular smooth muscle cells. *Endocrinology* **152**, 3143–3154 (2011).
- Kjøbsted, R. et al. AMPK in skeletal muscle function and metabolism. *FASEB J.* **32**, 1741–1777 (2018).
- Dagon, Y. et al. p70S6 kinase phosphorylates AMPK on serine 491 to mediate leptin's effect on food intake. *Cell Metab.* **16**, 104–112 (2012).
- Ovens, A. J. et al. Structure-function analysis of the AMPK activator SC4 and identification of a potent pan AMPK activator. *Biochem. J.* **479**, 1181–1204 (2022).
- Livingstone, R., Bryant, N. J., Boyle, J. G., Petrie, J. R. & Gould, G. W. Diabetes is accompanied by changes in the levels of proteins involved in endosomal GLUT4 trafficking in obese human skeletal muscle. *Endocrinol. Diab. Metab.* **5**, e361 (2022).
- Ramos, P. A. et al. Insulin-stimulated muscle glucose uptake and insulin signaling in lean and obese humans. *J. Clin. Endocrinol. Metab.* **106**, e1631–e1646 (2021).
- Sriwijitkamol, A. et al. Effect of acute exercise on AMPK signaling in skeletal muscle of subjects with type 2 diabetes: a time-course and dose-response study. *Diabetes* **56**, 836–848 (2007).
- Fujii, N. et al. Ablation of AMP-activated protein kinase $\alpha 2$ activity exacerbates insulin resistance induced by high-fat feeding of mice. *Diabetes* **57**, 2958–2966 (2008).
- Zhou, B. et al. Serum- and glucocorticoid-induced kinase drives hepatic insulin resistance by directly inhibiting AMP-activated protein kinase. *Cell Rep.* **37**, 109785 (2021).
- Myers, R. W. et al. Systemic pan-AMPK activator MK-8722 improves glucose homeostasis but induces cardiac hypertrophy. *Science* **357**, 507–511 (2017).
- Kjøbsted, R. et al. Intact regulation of the AMPK signaling network in response to exercise and insulin in skeletal muscle of male patients with type 2 diabetes: Illumination of AMPK activation in recovery from exercise. *Diabetes* **65**, 1219–1230 (2016).
- Suzuki, T. et al. Inhibition of AMPK catabolic action by GSK3. *Mol. Cell* **50**, 407–419 (2013).
- Park, D. W. et al. GSK3 β -dependent inhibition of AMPK potentiates activation of neutrophils and macrophages and enhances severity of acute lung injury. *Am. J. Physiol. Lung Cell Mol. Physiol.* **307**, L735–L745 (2014).

40. Heathcote, H. R. et al. Protein kinase C phosphorylates AMP-activated protein kinase alpha1 Ser487. *Biochem J.* **473**, 4681–4697 (2016).

41. Tonks, K. T. et al. Impaired Akt phosphorylation in insulin-resistant human muscle is accompanied by selective and heterogeneous downstream defects. *Diabetologia* **56**, 875–885 (2013).

42. Klip, A., McGraw, T. E. & James, D. E. Thirty sweet years of GLUT4. *J. Biol. Chem.* **294**, 11369–11381 (2019).

43. Bengal, E., Aviram, S. & Hayek, T. p38 MAPK in glucose metabolism of skeletal muscle: Beneficial or harmful? *Int J. Mol. Sci.* **21**, 6480 (2020).

44. Chambers, M. A., Moylan, J. S., Smith, J. D., Goodyear, L. J. & Reid, M. B. Stretch-stimulated glucose uptake in skeletal muscle is mediated by reactive oxygen species and p38 MAP-kinase. *J. Physiol.* **587**, 3363–3373 (2009).

45. Combes, A. et al. Exercise-induced metabolic fluctuations influence AMPK, p38-MAPK and CaMKII phosphorylation in human skeletal muscle. *Physiol. Rep.* **3**, e12462 (2015).

46. Gehart, H., Kumpf, S., Ittner, A. & Ricci, R. MAPK signalling in cellular metabolism: stress or wellness? *EMBO Rep.* **11**, 834–840 (2010).

47. Sylow, L. et al. Rac1 signaling is required for insulin-stimulated glucose uptake and is dysregulated in insulin-resistant murine and human skeletal muscle. *Diabetes* **62**, 1865–1875 (2013).

48. Bowers, S. L., Norden, P. R. & Davis, G. E. Molecular signaling pathways controlling vascular tube morphogenesis and pericyte-induced tube maturation in 3D extracellular matrices. *Adv. Pharm.* **77**, 241–280 (2016).

49. Batra, A. et al. Deletion of P21-activated kinase-1 induces age-dependent increased visceral adiposity and cardiac dysfunction in female mice. *Mol. Cell Biochem* **476**, 1337–1349 (2021).

50. Virtue, S. & Vidal-Puig, A. GTTs and ITTs in mice: simple tests, complex answers. *Nat. Metab.* **3**, 883–886 (2021).

51. Baskaran, Y. et al. An in cellulo-derived structure of PAK4 in complex with its inhibitor Inka1. *Nat. Commun.* **6**, 8681 (2015).

52. Khramushin, A. et al. Modeling beta-sheet peptide-protein interactions: Rosetta FlexPepDock in CAPRI rounds 38–45. *Proteins* **88**, 1037–1049 (2020).

53. London, N., Raveh, B., Cohen, E., Fathi, G. & Schueler-Furman, O. Rosetta FlexPepDock web server-high resolution modeling of peptide-protein interactions. *Nucleic Acids Res* **39**, W249–W253 (2011).

54. Koh, A. et al. Microbial imidazole propionate affects responses to metformin through p38 γ -dependent inhibitory AMPK phosphorylation. *Cell Metab.* **32**, 643–653.e644 (2020).

55. Ying, L. et al. Paracrine FGFs target skeletal muscle to exert potent anti-hyperglycemic effects. *Nat. Commun.* **12**, 7256 (2021).

(2023R1A2C3002389), all of which were funded by the Korean government. The funders had no role in study design, data collection and analysis, decision to publish or preparation of the manuscript.

Author contributions

DW and HCY performed the in vitro and in vivo experiments. HNC, SP, and SYP performed hyperinsulinemic-euglycemic clamp study. YL conducted computational simulation for the PAK4 phosphorylation of AMPK. SJY conducted the acquisition and analysis of human muscle tissues. BHP and EJB designed the experiments, interpreted the data, and wrote the manuscript. All authors reviewed the manuscript.

Competing interests

The authors declare no competing interests.

Additional information

Supplementary information The online version contains supplementary material available at <https://doi.org/10.1038/s41467-024-51240-w>.

Correspondence and requests for materials should be addressed to So-Young Park, Byung-Hyun Park or Eun Ju Bae.

Peer review information *Nature Communications* thanks the anonymous reviewers for their contribution to the peer review of this work. A peer review file is available.

Reprints and permissions information is available at <http://www.nature.com/reprints>

Publisher's note Springer Nature remains neutral with regard to jurisdictional claims in published maps and institutional affiliations.

Open Access This article is licensed under a Creative Commons Attribution-NonCommercial-NoDerivatives 4.0 International License, which permits any non-commercial use, sharing, distribution and reproduction in any medium or format, as long as you give appropriate credit to the original author(s) and the source, provide a link to the Creative Commons licence, and indicate if you modified the licensed material. You do not have permission under this licence to share adapted material derived from this article or parts of it. The images or other third party material in this article are included in the article's Creative Commons licence, unless indicated otherwise in a credit line to the material. If material is not included in the article's Creative Commons licence and your intended use is not permitted by statutory regulation or exceeds the permitted use, you will need to obtain permission directly from the copyright holder. To view a copy of this licence, visit <http://creativecommons.org/licenses/by-nc-nd/4.0/>.

© The Author(s) 2024, corrected publication 2025

Acknowledgements

This work was supported by grants from the Bio & Medical Technology Development Program (2022M3E5F2017607), Korea Drug Development Fund (HN21C0447), and Basic Science Research Program